Forward production of protons and pions in heavy-ion collisions

Rudolph C. Hwa[1] and Li-Lin Zhu[1,2]
[1]*Institute of Theoretical Science and Department of Physics, University of Oregon, Eugene, Oregon 97403-5203, USA*
[2]*Institute of Particle Physics, Hua-Zhong Normal University, Wuhan 430079, People's Republic of China*
(Received 18 June 2008; published 25 August 2008)

The problem of forward production of hadrons in heavy-ion collisions at RHIC is revisited with a modification of the theoretical treatment on the one hand and with the use of new data on the other. The basic formalism for hadronization remains the same as before, namely, recombination, but the details of momentum degradation and quark regeneration are improved. Recent data on the p/π and $\bar{p}/p$ ratios are used to constrain the value of the degradation parameter. The transverse momentum (p_T) spectrum of the average charged particles is well reproduced. A prediction on the p_T dependence of the $\bar{p}/p$ ratio at $\eta = 3.2$ is made.

DOI: 10.1103/PhysRevC.78.024907 PACS number(s): 25.75.Dw

I. INTRODUCTION

Theoretical study of hadron production in the forward direction in heavy-ion collisions is a difficult problem for several reasons. The empirical fact that the proton/pion ratio is large at large rapidity implies that neither fragmentation nor hydrodynamics can be successful in describing the process of hadron production in that region. Recombination is the natural hadronization mechanism for large baryon/meson ratio, but the parton momentum distribution at low Q^2 and large momentum fraction x (contributing to hadronic Feynman x_F in the range $0.3 < x_F < 1.0$) in nuclear collisions is hard to determine, especially when momentum degradation and soft-parton regeneration cannot be ignored. The use of data as input to constrain unknown parameters is unavoidable; however, that is also where further complexity arises. Data on forward production at $\eta = 3.2 \pm 0.2$ depend on both the longitudinal and transverse momenta, p_L and p_T, resulting in a smearing of the x distributions of the partons that makes phenomenology difficult owing to the interconnectedness of all aspects of the dynamical problem. The problem was first studied in the framework of the recombination model in Refs. [1–3] with the effects of parton regeneration taken into account [4,5]. The original data from PHOBOS show the distribution of charged particles at large η, but without a p_T measurement the value of x_F cannot be determined [6]. BRAHMS has measured both the η and p_T dependencies of charged hadrons [7], but without particle identification the p/π ratio cannot be inferred. Very recently, there are preliminary data that indicate the p/π ratio at $\eta = 3.2$ to be very large, $\sim$4 at $p_T = 1.1$ GeV/c and 0–10% centrality in Au-Au collisions at $\sqrt{s} = 62.4$ GeV [8], about three times higher than the prediction in Ref. [5]. The aim of this paper is to reexamine the problem of forward production and show that, with appropriate changes in the treatment of degradation, regeneration, and transverse momentum, the large p/π ratio in the fragmentation region can be understood.

In addition to the new data on the p/π ratio there is also a new presentation of the $\bar{p}/p$ ratio by BRAHMS for $\sqrt{s} = 62.4$ GeV, where the value of $R_{\bar{p}/p} \simeq 0.02$ is given [9]. That value differs from the value 0.05 inferred from the figure presented in Ref. [10], which was the value used in Ref. [5]. The new values of $R_{p/\pi}$ and $R_{\bar{p}/p}$ are consistent with the implication that there are more quarks or less antiquarks than what were obtained in Ref. [5]. This result provides a hint for us to look for an area in the formalism where the treatment of degradation and regeneration may be improved. Regeneration is an effect that depends on momentum degradation in forward propagation, which in turn depends on the degradation parameter κ, which is not known except by fitting the data. With new data available, the whole procedure needs to be revised. In this paper we change the strategy of our phenomenology to take advantage of the additional constraints provided by the particle ratios.

The formalism for forward production is basically the same as discussed in Refs. [4,5]. We describe its essence in Sec. II, but with special emphasis on changes that are necessary to improve the treatment. In Sec. III momentum degradation and quark regeneration are investigated with significant changes from Refs. [4,5]. How the data on particle ratio can be used to constrain κ is discussed in Sec. IV, followed by consideration of the transverse momentum in Sec. V. Conclusions are given in Sec. VI.

II. BASIC FORMALISM FOR FORWARD PRODUCTION

In the recombination model (RM) [1–3] hadron production can be described by the basic equations

$$H_p^{AB}(x) = \int \frac{dx_1}{x_1}\frac{dx_2}{x_2}\frac{dx_3}{x_3} F_{uud}^{AB}(x_1, x_2, x_3) R_p(x_1, x_2, x_3, x), \tag{1}$$

$$H_\pi^{AB}(x) = \int \frac{dx_1}{x_1}\frac{dx_2}{x_2} F_{q\bar{q}}^{AB}(x_1, x_2) R_\pi(x_1, x_2, x) \tag{2}$$

for protons and pions, respectively, where only a one-dimensional consideration is needed for forward production, with $x \equiv x_F = 2p_L/\sqrt{s}$ for hadrons and x_i being the momentum fractions of partons [4,5]. The recombination functions (RFs), R_p and R_π, depend on the wave functions of the hadrons and are summarized in Ref. [4]. The major task to render Eqs. (1) and (2) useful is to determine the parton distributions F_{uud}^{AB} and $F_{q\bar{q}}^{AB}$ for the problem at hand. For forward production

the largest contribution can be attained if the quarks arise from different initial nucleons so that their momenta do not have to be shared among the quarks originating from the same nucleon. That means $F^{AB}_{uud}(x_1, x_2, x_3)$ depends on a factorizable product of independent quark distributions $F^{\nu_i}_q(x_i)$ at momentum fraction x_i of an incident nucleon after ν_i collisions with the target nucleus B; similarly, $F^{AB}_{q\bar{q}}(x_1, x_2)$ involves quark and antiquark distributions. If only three or two nucleons in the projectile A are considered in each collision, we can define the p and π distributions from such sources as $H^{(3)B}_p$ and $H^{(2)B}_\pi$, which are then related to the overall distributions for AB collisions by

$$H^{AB}_p(x, b) = \int \frac{d^2s}{\sigma} \frac{[\sigma T_A(s)]^3}{3!} H^{(3)B}_p(x, b, s), \tag{3}$$

$$H^{AB}_\pi(x, b) = \int \frac{d^2s}{\sigma} \frac{[\sigma T_A(s)]^2}{2!} H^{(2)B}_\pi(x, b, s), \tag{4}$$

where b is the impact parameter. These formulas are derived in Ref. [4]. Clearly, to describe $H^{(3)B}_p$ and $H^{(2)B}_\pi$ is a simpler problem than in Eqs. (1) and (2), since the corresponding parton distributions are for three and two nucleons, respectively, in the projectile. In Eqs. (3) and (4) σ denotes the inelastic cross section of nucleon-nucleon collisions, and $T_A(s)$ is the thickness function for a tube in A at impact parameter s.

The recombination equation for the reduced projectile going through the target B is as in Eqs. (1) and (2)

$$H^{(3)B}_p(x, b, s) = \int \frac{dx_1}{x_1}\frac{dx_2}{x_2}\frac{dx_3}{x_3} F^{(3)B}_{qqq}(x_1, x_2, x_3; |\vec{s} - \vec{b}|) \times R_p(x_1, x_2, x_3, x), \tag{5}$$

$$H^{(2)B}_\pi(x, b, s) = \int \frac{dx_1}{x_1}\frac{dx_2}{x_2} F^{(2)B}_{q\bar{q}}(x_1, x_2; |\vec{s} - \vec{b}|) \times R_\pi(x_1, x_2, x), \tag{6}$$

where $F^{(3)B}_{qqq}(x_1, x_2, x_3; |\vec{s} - \vec{b}|)$ is the three-quark joint distribution after three nucleons transverse the target nucleus at impact parameter $|\vec{s} - \vec{b}|$ in B. We shall neglect the minor flavor dependence of nucleons and quarks in the following. Similarly, $F^{(2)B}_{q\bar{q}}(x_1, x_2; |\vec{s} - \vec{b}|)$ is the $q\bar{q}$ distribution after two nucleons go through B. In Ref. [4] $F^{(3)B}_{qqq}$ is assumed to have a factorizable form. We now give a derivation of that form and in the process determine the appropriate average number of collisions. The same follows for $F^{(2)B}_{q\bar{q}}$.

If each nucleon in the projectile nucleus A at $\vec{s}$ makes on average $\bar{\nu}$ collisions in B, where

$$\bar{\nu} \equiv \bar{\nu}^{pB}(|\vec{s} - \vec{b}|) = \frac{\sigma T_B(|\vec{s} - \vec{b}|)}{1 - \exp[-\sigma T_B(|\vec{s} - \vec{b}|)]}, \tag{7}$$

then three nucleons make on average $3\bar{\nu}$ collisions. Assuming a Poisson distribution in ν, we have

$$H^{(3)B}_p(x; b, s) = \sum_\nu H^{(3)B}_p(x; \nu) P_{3\bar{\nu}}(\nu), \tag{8}$$

where

$$P_{\bar{\nu}}(\nu) = \frac{\bar{\nu}^\nu}{\nu!} e^{-\bar{\nu}}. \tag{9}$$

By applying Eq. (8) to Eq. (5) the sum over ν can be moved past the integrals and we can write

$$F^{(3)B}_{qqq}(x_1, x_2, x_3; |\vec{s} - \vec{b}|) = \sum_\nu F^{(3)B}_{qqq}(x_1, x_2, x_3; \nu) P_{3\bar{\nu}}(\nu). \tag{10}$$

Now, ν is the total number of wounded nucleons experienced by the target nucleus B, irrespective of how it is distributed among the incident nucleons. With three such nucleons that are independent, we have

$$F^{(3)B}_{qqq}(x_1, x_2, x_3; \nu) = \frac{1}{3^\nu} \sum_{\nu_1,\nu_2,\nu_3} \frac{\nu!}{\nu_1!\nu_2!\nu_3!} F^{\nu_1}_q(x_1) F^{\nu_2}_q(x_2) F^{\nu_3}_q(x_3), \tag{11}$$

where the summation over ν_i is constrained by $\sum_i \nu_i = \nu$, each starting from $\nu_i = 0$. Each term in the summand is a product of single-quark distributions in a proton that has undergone ν_i collisions with the target. They include the effects of degradation and regeneration to be discussed in the following.

The use of $3\bar{\nu}$ in the Poisson distribution in Eq. (10) is based on the assumption that all three nucleons in the projectile are lined up in the same tube at impact parameter $|\vec{s} - \vec{b}|$ in B, since otherwise the forward partons are not nearby in the transverse plane and are unlikely to recombine to form a proton. Thus the same $\bar{\nu}^{pB}$ applies to each of the three nucleons. By substituting Eq. (11) into (10) and making use of the implicit $\delta_{\nu,\nu_1+\nu_2+\nu_3}$ contained in the summation in (11), the sum over ν can readily be carried out, yielding

$$F^{(3)B}_{qqq}(x_1, x_2, x_3; |\vec{s} - \vec{b}|) = \prod_{i=1}^{3} F^{\bar{\nu}}_q(x_i), \tag{12}$$

where

$$F^{\bar{\nu}}_q(x_i) = \sum_{\nu_i=0}^{\infty} F^{\nu_i}_q(x_i) P_{\bar{\nu}}(\nu_i), \tag{13}$$

with $\bar{\nu}$ being defined in Eq. (7) for pB collisions. Using Eq. (12) in Eq. (5) and then in Eq. (3) we have reduced the proton production problem in AB collisions to the only issue at hand [i.e., how the parton distribution $F^{\bar{\nu}}_q(x_i)$ is to be determined].

For forward production we ignore the production of resonances and their decays. A proton is in the symmetric state in SU(2) × SU(2) for (spin, isospin). In $2 \times 2 \times 2 = 4 + 2_a + 2_s$ for qqq, the symmetric state $(2_s, 2_s) + (2_a, 2_a)$ is 8 out of a total of 64 states, so the statistical factor $g_{\rm st}$ in $R_p(x_1, x_2, x_3, x)$ is 1/8. For the pion there is no change in $R_\pi(x_1, x_2, x)$ from that given in Ref. [4].

III. MOMENTUM DEGRADATION AND QUARK REGENERATION

The problem of forward production in pB collisions has been treated in the framework of the valon model, which connects the bound-state problem of a static proton (in terms of constituent quarks) with the structure problem of a proton

in collision (in terms of partons) [2,3,11]. Without momentum degradation the quark distribution in a free proton is given by

$$F_q(x_i, Q^2) = \int_{x_i}^{1} dy G(y) K\left(\frac{x_i}{y}, Q^2\right), \tag{14}$$

where $G(y)$ is the valon distribution, with y being the momentum fraction of the valon, and $K(z, Q^2)$ is the quark distribution in a valon, both of which have been parametrized and updated in Ref. [12]. With momentum degradation in proton-nucleus collisions both $G(y)$ and $K(z, Q^2)$ are modified, as described in Refs. [4,5]. However, we have come to the realization that Eq. (14) itself needs modification, a new development that we now describe from the beginning.

A proton has three valons, which are the constituent quarks in the bound-state problem. When a proton wounds ν nucleons in the target nucleus, it does not matter which of the three valons causes the wounding; they can act independently. It is important to recognize the possibility that one of the valons may not undergo any momentum degradation, while the other two are responsible for causing ν wounded nucleons in the target. Although the probability of that is low, the valence quark in the undegraded valon would have higher momentum. The point is that we should consider all possibilities, which can be expressed in the form

$$F_q^{\nu}(x_i) = \frac{1}{2^{\nu}} \sum_{\mu=0}^{\nu} \frac{\nu!}{\mu!(\nu-\mu)!} \int_{x_i}^{\kappa^{\mu}} dy' G_{\mu}'(y') K\left(\frac{x_i}{y'}\right), \tag{15}$$

where the Q^2 dependence, shown explicitly in Eq. (14), is suppressed because it is at some unspecified low value that is not of central importance here. $G_{\mu}'(y')$ is the modified valon distribution due to degradation to be discussed in the following, together with the upper limit of integration. The Poissonian averaging of μ, the number of nucleons in B wounded by a valon, allows μ to be zero, while the total number of wounded nucleons is fixed at ν. Thus the way that the valons are treated in a projectile nucleon is analogous to the way that the nucleons are treated in a projectile nucleus.

If the momentum fraction that a valon retains after a collision with a nucleon in B is κ, then after μ collisions the modified valon distribution is

$$y' G_{\mu}'(y') = \int_{y'}^{1} dy G(y) \kappa^{\mu} \delta\left(\frac{y'}{y} - \kappa^{\mu}\right), \tag{16}$$

which satisfies the normalization condition

$$\int dy' G_{\mu}'(y') = \int dy G(y) = 1. \tag{17}$$

The solution of Eq. (16) is

$$G_{\mu}'(y') = \kappa^{-\mu} G\left(\kappa^{-\mu} y'\right). \tag{18}$$

It is clear that the maximum value of y' is κ^{μ} because of the μ-fold degradation, thus setting the upper limit of integration in Eq. (15). Furthermore, the average momentum of the degraded valon is

$$\langle y' \rangle_{\mu} = \int dy' y' G_{\mu}'(y') = \kappa^{\mu} \langle y \rangle = \frac{1}{3} \kappa^{\mu}, \tag{19}$$

where $\langle y \rangle$ is the average momentum fraction of a valon in a free proton and is 1/3. Thus Eq. (19) expresses the effect of degradation in this simple model of multiplicative momentum loss of the sequential collision process.

The valence quark distribution in a proton after ν collision is as expressed in Eq. (15), but with $K(z)$ replaced by the nonsinglet component $K_{\rm NS}(z)$, which is specified in Ref. [12]. Owing to the μ dependence of $G_{\mu}'(y')$ in Eqs. (18) and (19), the sum over μ in Eq. (15) acquires special significance at low μ, as remarked earlier before that equation. It is the $\mu = 0$ term that renders the valence quark distribution at intermediate x_i insensitive to the value of κ. In this respect our treatment here is an improvement over that in Refs. [4,5].

For the regenerated sea quark distributions the earlier treatment can also be improved. In Ref. [5] the quark distribution $K(z)$ in a valon is written in the two-component form

$$K(z) = K_{\rm NS}(z) + L''(z), \tag{20}$$

where $L''(z)$ represents the regenerated sea quark distribution in a valon, including gluon conversion. The regenerated $\bar{q}$ distribution, $F_{\bar{q}}^{\nu}(x_i)$, for a nucleon making ν collisions with the target is then as given in Eq. (15), but with $K(z)$ replaced by $L''(z)$. We now realize that such a convolution equation gives only a part of the total $\bar{q}$ distribution because the momentum lost by a nucleon after ν collisions is not totally accounted for by that convolution equation. The average momentum loss of a nucleon as a fraction of the initial momentum after ν collisions is $1 - \langle x \rangle_{\nu}$, where

$$\langle x \rangle_{\nu} = \frac{1}{3^{\nu}} \sum_{\mu_1,\mu_2,\mu_3} \frac{\nu!}{\mu_1!\mu_2!\mu_3!} \kappa^{\mu_1} \kappa^{\mu_2} \kappa^{\mu_3} = \kappa^{\nu}. \tag{21}$$

We assume that the momentum loss is converted totally to $q\bar{q}$ pairs with q being u and d, but not s, which is suppressed because of the higher mass of the strange quark. Thus the regenerated $\bar{q}(\bar{u}$ or $\bar{d})$ distribution for each nucleon in the projectile, $F_{\bar{q}}^{\nu}(x)$, should satisfy the sum rule (with the subscript i on x_i suppressed)

$$\int dx F_{\bar{q}}^{\nu}(x) = \frac{1}{4}(1 - \kappa^{\nu}). \tag{22}$$

We adopt the approximate form for the x dependence:

$$F_{\bar{q}}^{\nu}(x) = f_{\nu}(1-x)^n, \tag{23}$$

so $f_{\nu} = (1 - \kappa^{\nu})/4(n+1)$. We shall use $n = 7$, since that is suggested by the $\bar{q}$ parton distribution of a free nucleon for x not too small and at low Q^2. For the values of κ and ν that we encounter in the following, Eq. (23) gives values of $F_{\bar{q}}^{\nu}(x)$, for $x > 0.2$, far greater than those obtained by the convolution of $G_{\nu}'(y')$ with $L''(x/y')$, as determined in Ref. [5]; the latter is therefore neglected hereafter.

To summarize, for quark (u or d) distributions in pB collisions after ν wounded nucleons in B, we have

$$F_q^{\nu}(x) = F_{q_v}^{\nu}(x) + F_{\bar{q}}^{\nu}(x), \tag{24}$$

where $F_{q_v}^{\nu}(x)$ is the valence quark distribution given by Eq. (15) with $K_{\rm NS}(z)$ in place of $K(z)$, and $F_{\bar{q}}^{\nu}(x)$ is the regenerated quark distribution given by Eq. (23). The antiquark distribution is, of course, just the second term in Eq. (24).

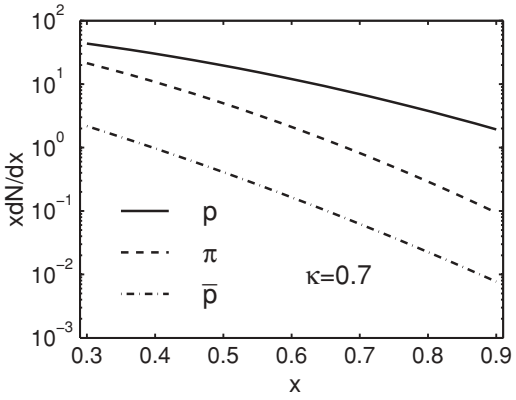

FIG. 1. The x distributions of produced protons, pions, and antiprotons in Au-Au collisions for $b = 3.3$ fm, $\sqrt{s} = 62.4$ GeV, and $\kappa = 0.7$.

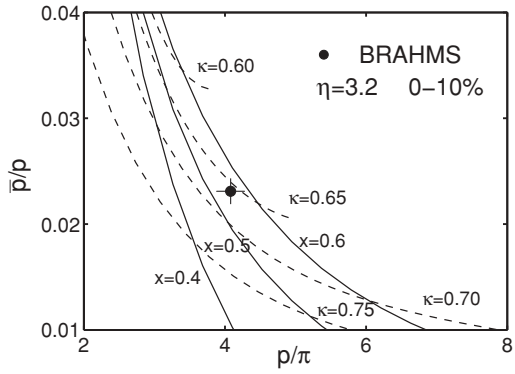

FIG. 2. A plot of the antiproton/proton ratio vs the proton/pion ratio for various fixed values of x (solid lines) and κ (dashed lines) for Au-Au collisions at 0%–10% centrality. The theoretical curves are determined by calculating $H_{h'}(x,\kappa)/H_h(x,\kappa)$. The experimental point is from the BRAHMS data on $R_{\bar{p}/p}$ [9] and $R_{p/\pi}$ [8] at $\sqrt{s} = 62.4$ GeV and $\eta = 3.2 \pm 0.2$.

IV. PARTICLE RATIOS

Having obtained the modified quark distribution resulting from degradation and regeneration, we can now use Eq. (24) in Eq. (13) for the ith nucleon, and then in Eq. (12) for qqq distribution emerging from three nucleons colliding with target B at impact parameter $|\vec{s} - \vec{b}|$. That result can then be used in Eqs. (3) and (5) to determine the x distribution of produced protons in AB collisions. Exactly the same procedure can be followed to obtain the spectra of π and $\bar{p}$ with appropriate use of the the $\bar{q}$ distribution for $q\bar{q}$ and $\bar{q}\bar{q}\bar{q}$ recombination.

We show in Fig. 1 the results of our calculation of the x distributions of p, π, and $\bar{p}$ for $\kappa = 0.7$ and $b = 3.3$ fm at 0%–10% centrality in Au-Au collisions. The value of κ is chosen for reasons to be given in the following. Evidently, the p distribution is much higher than the other two for $x > 0.5$, since it is due to the recombination of three valence quarks from three different nucleons in the projectile A. Moreover, it decreases more slowly with increasing x owing to the slower decrease of valence quark distribution compared to the sea quarks. Thus the p/π ratio is large and increases with increasing x. The π distribution is much higher than the $\bar{p}$ distribution, because of the effect of the valence quark in the pion that is lacking in the antiproton. Similar plots can also be made for other values of κ, but in the absence of any data on the hadronic x distributions the comparison among different κ values can better be presented in a different format, as shown in the following. The general trend is that lower κ leads to a higher level of $\bar{q}$ and therefore a higher π and $\bar{p}$ at low x.

Recently, data have become available on the particle ratios of both $\bar{p}/p$ [9] and p/π [8]. It is then very revealing for us to make parametric plots of those ratios for various values of x and κ. We use Eqs. (1) and (2) to calculate $H_h^{AB}(x,\kappa)$ for $b = 3.3$ fm and $h = p, \pi, \bar{p}$ and show their ratios $H_{\bar{p}}/H_p$ versus H_p/H_π in Fig. 2, in which the grid lines are for constant x (in solid lines) and constant κ (in dashed lines). It is clear that all lines have negative slopes in that figure because $\bar{q}$ is involved in the numerator of $H_{\bar{p}}/H_p$, but in the denominator of H_p/H_π. Large values of H_p/H_π can be achieved only when $x > 0.4$. That is the region where the valence quarks dominate and the sea quarks are suppressed. At fixed x both ratios depend sensitively on κ, more so for $H_{\bar{p}}/H_p$ than for H_p/H_π, because of the number of $\bar{q}$ involved. The smaller κ is, the more degradation there is, and the regenerated $\bar{q}$ boosts $H_{\bar{p}}/H_p$ and suppresses H_p/H_π.

The data on $R_{\bar{p}/p}$ and $R_{p/\pi}$ depend on the values of p_T at which the hadrons are included in the determination of the ratios. $R_{h'/h}$ cannot be identified with $H_{h'}/H_h$ until after the p_T distribution is considered, a topic to be discussed in the next section. So far we have only treated the dynamical processes that lead to the x distributions. At fixed η the longitudinal and transverse momenta are, of course, not kinematically independent. The range of x that is phenomenologically relevant to our study should correspond to the range of p_T in which the experimental values of the particle ratios are determined. Since the mismatch between $R_{h'/h}$ and $H_{h'}/H_h$ is not large, as we shall discuss later, let us here mark on Fig. 2 the data point that corresponds to [8,9]

$$R_{p/\pi} = 4.08 \pm 0.2, \quad \eta = 3.2 \pm 0.2, \quad 0.9 < p_T < 1.3\,\text{GeV}/c, \tag{25}$$

$$R_{\bar{p}/p} = 0.0231 \pm 0.0012, \quad y = 3.0 \pm 0.1, \quad 0.5 < p_T < 1.4\,\text{GeV}/c. \tag{26}$$

The grid lines in Fig. 2 then suggest that the relevant values of x and κ are

$$x \simeq 0.55 \quad \text{and} \quad \kappa \simeq 0.67. \tag{27}$$

For that reason the x distributions in Fig. 1 are shown for $\kappa = 0.7$.

What we have done so far is essentially the first step of an iteration process, in which the focus is on the x distribution. The next step is to consider the transverse momentum based on the result of the first step and to improve on the overall phenomenology.

V. TRANSVERSE MOMENTUM

The p_T dependence of the produced particles has been discussed in Ref. [5]. Let us first give a summary of that discussion. Since hard scattering is suppressed in the fragmentation region, we ignore shower partons for $x > 0.2$. This approximation is supported by the data on the p_T distribution of charged particles at $\eta = 3.2$ [7], which shows an exponential behavior for p_T up to 2 GeV/c without up-bending due to power-law behavior. Thus we write the x and p_T distributions of a produced hadron h in the factorizable form

$$\frac{x}{p_T}\frac{dN_h}{dx dp_T} = H_h(x,\kappa)V_h(p_T), \tag{28}$$

where the transverse part is normalized by

$$\int_0^\infty dp_T\, p_T V_h(p_T) = 1, \tag{29}$$

rendering

$$x\frac{dN_h}{dx} = H_h(x,\kappa), \tag{30}$$

which is our starting point in Eqs. (1) and (2).

The properties of $V_h(p_T)$ described in Ref. [5] are adapted from the treatment of p_T distribution in central collisions at mid-rapidity for which the only recombination process is in the transverse plane [13]. Here, we have treated in detail the degradation, regeneration, and recombination of partons in the forward production, so it is inappropriate to append a separate recombination of thermal partons with independent recombination functions for the transverse component. Since no shower partons are involved, we shall simply take a common exponential form for all hadrons but allow the inverse slopes T_h to differ for hadrons with different masses, as suggested by hydrodynamical flow. Thus we write

$$V_h(p_T) = \frac{1}{2T_h^2}e^{-p_T/T_h}, \tag{31}$$

with normalization chosen to satisfy Eq. (29). We parametrize T_h by

$$T_h = T_0 + m_h\langle v_t\rangle^2, \tag{32}$$

where the second term expresses the flow contribution. Since at large x the dominant momentum direction is longitudinal, the mass-dependent component of the transverse momentum is expected to be small compared to the thermal component characterized by T_0.

Although x and p_T appear to be independent in Eq. (28), they are kinematically constrained when η is fixed. They are related by

$$x = \frac{2p_T}{\sqrt{s}}\sinh\eta. \tag{33}$$

At $\eta = 3.2$, the range $1 \leqslant p_T \leqslant 1.5$ GeV/c corresponds to $0.39 \leqslant x \leqslant 0.59$. However, if the rapidity y is fixed, the relationship depends on the particle mass. At $y = 3.0$, the range $1 \leqslant p_T \leqslant 1.5$ GeV/c corresponds to $0.32 \leqslant x_\pi \leqslant 0.48$ and $0.44 \leqslant x_p \leqslant 0.57$. The value $x \simeq 0.55$ determined from our theoretical grid lines in Fig. 2 lies within the range of x values above for the data on $R_{p/\pi}$ at $\eta = 3.2$ in Eq. (25) and also within the range of x_p values above for the data on $R_{\bar{p}/p}$ at $y = 3.0$ in Eq. (26). This is a nontrivial achievement, since the formalism described in Sec. III makes no reference to p_T, so the grid lines for the ratios of $H_{h'/h}(x,\kappa)$ at constant κ and x need not imply any p_T values that correspond to the relevant x and p_T values of the experimental $R_{h'/h}$ at fixed η.

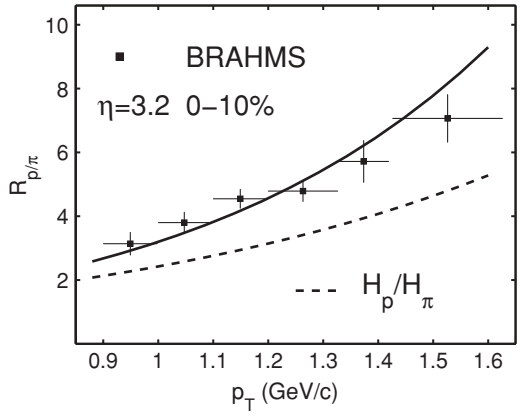

FIG. 3. The p_T dependence of the proton/pion ratio in Au-Au collisions at $\eta = 3.2$. The dashed line is obtained from the ratio $H_p[x(p_T)]/H_\pi[x(p_T)]$ with $\kappa = 0.67$. The solid line includes the factor $V_p(p_T)/V_\pi(p_T)$. The data (preliminary) are from Ref. [8].

The p_T distribution given in Ref. [7] is to be identified with our calculation as follows:

$$\frac{dN}{2\pi p_T dp_T d\eta} = \frac{1}{2\pi}H_h(x)V_h(p_T), \tag{34}$$

since upon integration over $p_T dp_T d\phi$ and by using Eq. (29) it yields $H_h(x)$. Strictly speaking, holding η fixed on the left-hand side is not the same as holding x fixed on the right-hand side. But the data are analyzed at $\eta = 3.2 \pm 0.2$, so there are bands of η and x values in which Eq. (34) is approximately valid. The data on $R_{p/\pi}(p_T)$ are then to be related to our calculation by

$$R_{p/\pi}(p_T) = \frac{H_p[x(p_T)]}{H_\pi[x(p_T)]}\frac{V_p(p_T)}{V_\pi(p_T)}, \tag{35}$$

where the ratio H_p/H_π is to be determined by fixing $\eta = 3.2$ and $\kappa = 0.67$. In Fig. 3 we show that ratio by the dashed line, which has a significant p_T dependence. Furthermore, the average magnitude of H_p/H_π accounts for the major part of $R_{p/\pi}$, and it cannot arise without a realistic treatment of degradation and regeneration. The reason for the dashed line to increase with p_T is that at fixed η higher p_T means higher x, where $\bar{q}$ is suppressed compared to q, resulting in π being suppressed relative to p. The solid line in Fig. 3 includes the effect of V_p/V_π, which we get from Eqs. (31) and (32):

$$\frac{V_p(p_T)}{V_\pi(p_T)} = \left(\frac{T_\pi}{T_p}\right)^2 \exp\left[-p_T\left(\frac{1}{T_p} - \frac{1}{T_\pi}\right)\right]. \tag{36}$$

Since the $m_h\langle v_t\rangle^2$ term in Eq. (32) is small compared to T_0, as we shall show presently, this ratio is approximately $\exp[(m_p - m_\pi)p_T\langle v_t\rangle^2/T_0^2]$, which shows the effect of mass difference in elevating the dashed line to the solid line. The result of fitting

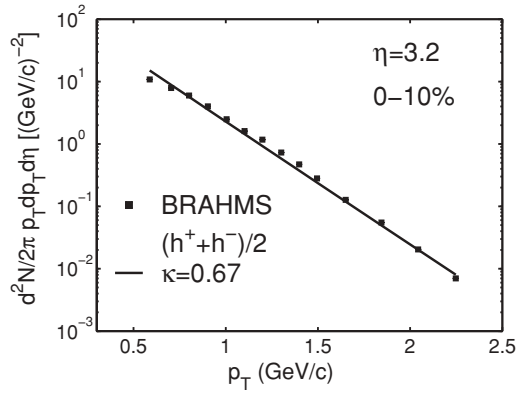

FIG. 4. The p_T distribution of average charged hadrons in Au-Au collisions at $\eta = 3.2$. The data are from Ref. [7]. The solid line is obtained by use of Eq. (34) for $h^{\pm} = [p + \bar{p} + 1.2(\pi^+ + \pi^-)]/2$ and $\kappa = 0.67$.

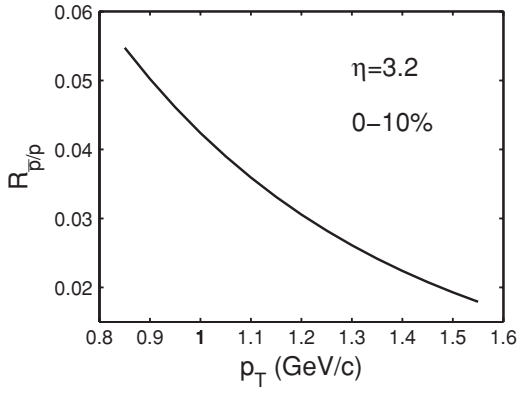

FIG. 5. The p_T dependence of the antiproton/proton ratio at 0%–10% centrality in Au-Au collisions for $\sqrt{s} = 62.4$ GeV, $\eta = 3.2$, and $\kappa = 0.67$.

the data [8] gives

$$\langle v_t \rangle^2 / T_0^2 = 0.7\,(\mathrm{GeV}/c)^{-2}. \tag{37}$$

This is consistent with $m_p \langle v_t \rangle^2 \ll T_0$, when T_0 is 0.2 GeV/c (to be determined in the following).

The p_T distribution itself is an additional test of our model, since the absolute normalization is not canceled as in a ratio. The data [7] are for all charged hadrons without particle identification, for which we treat $(h^+ + h^-)/2$ as $h^{\pm} = [p + \bar{p} + 1.2(\pi^+ + \pi^-)]/2$, where a K/π ratio of $\simeq$0.2 is used [9]. As the third step in our iteration process, we calculate $H_{h^{\pm}}(x) V_{h^{\pm}}(p_T)/2\pi$, holding x and κ fixed as in Eq. (27), and adjust T_0 to fit the data according to Eq. (34). The result is shown in Fig. 4 for $T_0 = 200$ MeV; it agrees with the data very well. Since the normalization is fixed by the $H_h(x, \kappa)$ functions and is not adjustable, a good fit is remarkable.

Putting the obtained value of T_0 in Eq. (37), we have

$$T_0 = 0.2\,\mathrm{GeV}/c, \quad \langle v_t \rangle^2 = 0.028. \tag{38}$$

The value of $\langle v_t \rangle \simeq 0.17$ seems reasonable in view of the dominance of longitudinal expansion in the fragmentation region. The significance of this work is, of course, not in the transverse aspect of the problem, but in the longitudinal momentum distributions of the forward particles, which affect the p_T distribution. The large p/π ratio found in the BRAHMS data at $\eta = 3.2$ cannot be understood without a proper treatment of the x distributions in the fragmentation region.

As a prediction of this work, we can calculate the p_T dependence of the $\bar{p}/p$ ratio at fixed $\eta = 3.2$. Since $V_{\bar{p}}/V_p = 1$ for $h = \bar{p}, p$, only $H_h[x(p_T)]$ contributes to the ratio $R_{\bar{p}/p}(p_T)$. Using Eq. (33), we have

$$R_{\bar{p}/p}(p_T) = \frac{H_{\bar{p}}[x(p_T)]}{H_p[x(p_T)]}. \tag{39}$$

The result for $\sqrt{s} = 62.4$ GeV, $b = 3.3$ fm, and $\kappa = 0.67$ is shown in Fig. 5. The range of p_T values covered by the plot corresponds to x roughly between 0.3 and 0.6 at $\eta = 3.2$. Note that the result is for fixed η, not fixed y. The reason for the decrease of $R_{\bar{p}/p}(p_T)$ with increasing p_T is clearly the increase of x, where $\bar{q}$ at momentum fraction x_i, approximately $x/3$, becomes more suppressed than q at the same x_i. A verification of this prediction would lend further support to our model.

VI. CONCLUSION

This work differs from the earlier attempt in Ref. [5] in three important ways. First, new data are available that put more stringent constraints on unknown parameters. Second, significant modifications have been made in the treatment of degradation, regeneration, and transverse momenta. Third, the order that phenomenology is carried out is reversed owing to the new empirical knowledge about the particle ratios. Using p/π and $\bar{p}/p$ ratios as input, we are able to determine the degradation parameter κ, which enables us to calculate the x distributions of the hadrons. At fixed η that implies a p_T dependence of the p/π ratio arising from the x distributions; that p_T dependence accounts for a large part of the data on that ratio, the balance being due to the exponential p_T distributions that are mass dependent. In fitting the particle ratio the calculated result is insensitive to the absolute normalization of the yield. The latter is shown to be correct when we succeed in reproducing the p_T spectrum of the average charged particle. That is a significant achievement because the yields of protons, pions, and antiprotons at large η depend strongly on the dynamical process of momentum degradation and soft-parton regeneration.

Although the degradation parameter κ is determined by data fitting, to get the spectra correctly for all hadrons through one such parameter relies on the validity of the treatment of the various subprocesses. Our results suggest that our model has captured the essence of the dynamics involved. In particular, the large p/π ratio would not have emerged from our calculation if recombination has not been used as the mechanism for hadronization.

Since proton production at large x is due to the recombination of three valence quarks from three nucleons in the projectile, in which there are numerous other valence quarks from other nucleons, we do not expect the events triggered by a large-x proton would have correlated partners distinguishable from the background. In that respect the hadronization problem is similar to that at intermediate p_T in heavy-ion collisions

at LHC, where so many semihard jets are produced that shower partons are dense and can recombine with large p/π ratio [14]. For the same reason as at large x studied here, it was also predicted that for triggers in the $10 < p_T < 20$ GeV/c range no correlation structure of associated particles would be found. Thus to a certain extent what we can learn about forward production at RHIC may reveal some aspects of the characteristics of what may be observed at intermediate p_T at midrapidity at LHC.

ACKNOWLEDGMENTS

We are grateful to I. C. Arsene, P. Staszel, F. Videbaek, and C. B. Yang for helpful communications. This work was supported, in part, by the U. S. Department of Energy under Grant No. DE-FG02-96ER40972 and by the National Science Foundation in China under Grant No. 10775057 and by the Ministry of Education of China under Grant No. 306022 and Project No. IRT0624.

[1] K. P. Das and R. C. Hwa, Phys. Lett. **B68**, 459 (1977).
[2] R. C. Hwa, Phys. Rev. D **22**, 759 (1980); **22**, 1593 (1980).
[3] R. C. Hwa and C. B. Yang, Phys. Rev. C **66**, 025205 (2002).
[4] R. C. Hwa and C. B. Yang, Phys. Rev. C **73**, 044913 (2006).
[5] R. C. Hwa and C. B. Yang, Phys. Rev. C **76**, 014901 (2007).
[6] B. B. Back *et al*. (PHOBOS Collaboration), Phys. Rev. Lett. **91**, 052303 (2003); **87**, 102303 (2001).
[7] I. C. Arsene *et al*. (BRAHMS Collaboration), nucl-ex/0602018.
[8] N. Katryska and P. Staszel (BRAHMS Collaboration), poster presentation at Quark Matter 2008, Jaipur, India, 4–10 February 2008, arXiv: 0806.1162.
[9] I. C. Arsene (BRAHMS Collaboration), talk presented at Quark Matter 2008, Jaipur, India, 4–10 February 2008, arXiv: 0806.0745.
[10] H. Yang (BRAHMS Collaboration), Czech. J. Phys. **56**, A27 (2006).
[11] R. C. Hwa and C. B. Yang, Phys. Rev. C **65**, 034905 (2002).
[12] R. C. Hwa and C. B. Yang, Phys. Rev. C **66**, 025204 (2002).
[13] R. C. Hwa and C. B. Yang, Phys. Rev. C **70**, 024905 (2004).
[14] R. C. Hwa and C. B. Yang, Phys. Rev. Lett. **97**, 042301 (2006).